JOURNAL OF SPACECRAFT AND ROCKETS
Vol. 47, No. 3, May–June 2010

Physical and Numerical Aspects of Simulating Rarefied Hypersonic Wedge Flow

Wilson F. N. Santos*
National Institute for Space Research, 12630-000 Cachoeira Paulista, Brazil

DOI: 10.2514/1.47875

This paper presents numerical simulations of truncated wedges in rarefied hypersonic flow. The impact of the geometric bluntness, dictated by heating, handling, or manufacturing requirements, on the aerodynamic heating has been investigated by employing the direct simulation Monte Carlo method. The results presented highlight the sensitivity of the heat transfer coefficient to changes on the frontal-face thickness of the leading edges. Some significant differences on the heat transfer coefficient provided by the direct simulation Monte Carlo method and by the free-molecular-flow equation were noted along the body surface at the immediate vicinity of the frontal-face/afterbody junction for the leading edges with thickness Knudsen numbers of 100, 10, and 1. It was found that the heat transfer rate for the smallest frontal-face thickness approached the free-molecular limit from above, whereas that obtained for the largest frontal-face thickness approached from below. The flowfield behavior and its influence on the heat transfer coefficient was investigated by using a model that classifies the molecules in three distinct classes: 1) undisturbed freestream, 2) reflected from the body surface, and 3) scattered (that is, molecules that had been indirectly affected by the presence of the leading edge). According to the results, for the conditions investigated, there is a particular frontal-face thickness that represents the crossover point in which the approach to the free-molecular limit is at the level of the free-molecular limit.

Nomenclature

C_h	=	heat transfer coefficient
d	=	molecular diameter, m
H	=	body height at the base, m
Kn	=	Knudsen number, λ/l
L	=	body length, m
l	=	characteristic length, m
M	=	Mach number
m	=	molecular mass, kg
N	=	number flux, $\mathrm{m}^{-2}\,\mathrm{s}^{-1}$
N_f	=	dimensionless number flux, $N/n_\infty V_\infty$
n	=	density number, m^{-3}
p	=	pressure, $\mathrm{N/m}^2$
q	=	heat flux, $\mathrm{W/m}^2$
R	=	circular cylinder radius, m
Re	=	Reynolds number, $\rho V l/\mu$
S	=	dimensionless arc length, s/λ_∞
s	=	arc length, m
T	=	temperature, K
t	=	frontal-face thickness, m
V	=	velocity, m/s
X, Y	=	x and y normalized by λ_∞
x, y	=	Cartesian axes in physical space, m
η	=	coordinate normal to body surface, m
θ	=	wedge half-angle, deg
λ	=	mean free path, m
μ	=	viscosity, $\mathrm{Ns/m}^2$
ξ	=	coordinate tangent to body surface, m
ρ	=	density, $\mathrm{kg/m}^3$
χ	=	mole fraction
ω	=	viscosity index

Subscripts

t	=	relative to frontal-face thickness
w	=	wall conditions
1	=	relative to molecular class 1
2	=	relative to molecular class 2
3	=	relative to molecular class 3
∞	=	freestream conditions

I. Introduction

IN TYPICAL aerospace missions, vehicle performance is directly related to the aerodynamic characteristics of the design. In particular, the lift-to-drag L/Dratio indicates one aspect of the aerodynamic efficiency of the vehicle. One class of aerospace vehicles that have shown the ability to attain a higher L/D ratio compared to conventional vehicle designs is waveriders. Waverider configurations, introduced by Nonweiler [1], are derived from a known analytical flowfield, such as flow over a two-dimensional wedge or flow around a slender cone. These configurations are designed analytically with infinitely sharp leading edges for shock wave attachment. The attached shock wave eliminates flow leakage from the high-pressure lower surface to the upper surface, resulting in the potential for a high L/D ratio.

It has long been known that a very sharp leading edge is not practical for a number of reasons. The most important of them are related to manufacturing, handling, and heating requirements. It is extremely difficult to construct a perfectly sharp leading edge. Even with the most efficient and careful fabrication process, the leading edges will be several microns thick. In this fashion, for waverider configurations, any manufacturing error may result in a significant deviation from the original design contour. In addition to that, sharp edges are difficult to maintain because they are easily damaged. Moreover, sharp leading edges are associated with high aerodynamic heating because the heat flux to the leading edge varies inversely with the square root of the leading-edge nose radius. Therefore, for either manufacturing, handling, or heating concerns, a hypersonic leading edge should be blunt. Nevertheless, a blunt leading edge promotes shock wave detachment, making leading-edge blunting a major concern in the design and prediction of flowfields for hypersonic waverider configurations.

To account for any difficulties in manufacturing technology because of the impossibility to achieve in practice sharp leading

Received 28 October 2009; revision received 21 December 2009; accepted for publication 7 January 2010.

*Researcher, Combustion and Propulsion Laboratory. Member AIAA.

edges on airframes, Santos [2] has investigated the effect of the frontal-face thickness on the flowfield structure and on the aerodynamic surface quantities over truncated wedges. The emphasis of the work was to provide a critical analysis on maximum allowable geometric bluntness, dictated by either heat transfer or manufacturing requirements, resulting in reduced departures from ideal aerodynamic performance of the hypersonic vehicle, thus allowing the blunted leading edge to more closely represent the original sharp leading-edge flowfield. The frontal-face thickness impact on the aerodynamic surface quantities was investigated for thickness defined by 0.01, 0.1, and 1 times the freestream molecular mean free path, which corresponded to thickness Knudsen numbers of 100, 10, and 1, respectively. Therefore, based on the frontal-face thickness, this Knudsen number range covered from the transitional-flow regime to the free-molecular-flow one. In such an intermediate flow regime, the complete investigation of the flowfield structure was obtained by the direct simulation Monte Carlo (DSMC) method.

Santos [3] extended the analysis presented by Santos [2] on truncated wedges by performing a parametric study on these shapes, with emphasis placed on the compressibility effects. The primary goal was to assess the sensitivity of the shock wave standoff distance, stagnation-point heating, and total drag to changes on the freestream Mach number.

Santos [4] extended further the previous analysis on truncated wedges by examining the impact of the angle of attack on the aerodynamic surface quantities acting on the leading edges under hypersonic transitional-flow conditions. Of particular interest in the analysis was the aerodynamic performance of the leading edges, because blunt leading edges at incidence allow leakage of the high-pressure lower-surface flow into the upper-surface region, causing a reduction in the lift as well as on the L/D ratio. The analysis verified that even the leading edge with the smallest frontal-face thickness investigated, Kn_t of 100, resulted in a significantly reduction on the L/D ratio. The investigation was of great importance because it is impossible to achieve ideally sharp leading edges of airframes, such as waveriders.

Of particular interest in the analysis carried out by Santos [2,3] was the heat transfer coefficient behavior. It was somewhat surprising to find that for the thickness Knudsen number of 100, the heat transfer coefficient was above that predicted by the free-molecular-flow equations at the immediate vicinity of the frontal-face/afterbody junction on the afterbody surface. In contrast, the heat transfer coefficient for thickness Knudsen number of 1 was below that predicted by the free-molecular flow at the same station.

According to the literature [5–15], a similar behavior has been observed on the aerodynamic surface properties at the vicinity of the nose for sharp leading edges, such as flat plate, wedge, and cone. For the purpose of this introduction, it will be sufficient to describe only a few of these research studies.

Pan and Probstein [5] investigated the aerodynamic surface quantities on flat plates by considering rarefied flow. Their solution showed that the heat transfer rate could be greater than that predicted by the free-molecular value and that with decreasing Reynolds number the heat transfer curve would approach the free-molecular value from above.

Vidal and Bartz [6] observed from their experimental investigations on flat plates and wedges that the heat transfer rate approached the free-molecular limit from above, whereas those obtained at large wedge angles approached from below. According to them, for the particular conditions on the experiment, a 2 deg wedge angle appeared to be the crossover point in which the approach to the free-molecular limit was at the level of the free-molecular limit. Their wedge flows were produced by pitching the flat-plate model to various compression angles.

In the present account, effort is directed to understand the flowfield behavior on the truncated wedges [2,3] and its influence on the heat transfer coefficient, at the vicinity of the frontal-face/afterbody junction, in comparison to that yielded by the free-molecular-flow analysis. In pursuit of this goal, an approach based on the physics of the particles will be employed.

II. Body-Shape Definition

The geometry of the leading edges in this work is the same as that presented in previous studies [2,3]. The truncated wedges are modeled by assuming a sharp-edged wedge of half-angle θ with a circular cylinder of radius R inscribed tangent to this sharp leading edge. The truncated wedges are also tangent to the sharp-edged wedge and the cylinder at the same common point. A leading-edge half-angle of 10 deg, a circular cylinder diameter of 10^{-2} m, and frontal-face thickness t/λ_∞ of 0.01, 0.1, and 1, where λ_∞ is the freestream mean free path, were assumed. Figure 1 illustrates schematically this construction.

III. Computational Tool

The characteristic parameter that determines gas flow properties is the Knudsen number $Kn = \lambda/l$, where λ is the molecular mean free path and l is the reference flow scale. In the continuum-flow regime, as the Knudsen number tends toward zero, microscopic structure can be ignored, and a system can be completely described in terms of the macroscopic parameters, such as velocity, density, pressure, and temperature. In the free-molecular-flow regime, as the Knudsen number tends toward infinity, collisions between molecules can be neglected, and the flow behavior is determined by interactions between molecules and boundary surfaces. The region between the continuum and free-molecular-flow regimes is called the transitional-flow regime. In the transitional-flow regime, where the microscopic structure cannot be neglected, viscosity, heat conduction, relaxation, diffusion, and chemical processes are important. In this flow regime, the Knudsen number is of the order of unity.

The governing equation in the transitional-flow regime is the transport Boltzmann equation [16]. It is a nonlinear integral-differential equation, closed with respect to the one-particle distribution function, which in turn determines the density of particles in a six-dimensional phase space of particle coordinates and velocities. To circumvent the difficulty of a direct solution of the Boltzmann equation, the DSMC method [17] has been the approach of choice for the study of complex multidimensional flows of rarefied hypersonic aerothermodynamics.

The DSMC method [17] models a gas flow by using a computer to track the trajectory of simulated particles, where each simulated particle represents a fixed number of real gas particles. The simulated particles are allowed to move and collide, while the computer stores their positions, velocities, and other physical properties, such as internal energy. The DSMC method consists of four primary steps: molecular movements, indexing and cross-referencing molecules, molecular collisions, and flowfield sampling. The molecular movement process is modeled deterministically, whereas molecular collision is a probabilistic process. Figure 2 illustrates a simple DSMC algorithm for a steady-state flow simulation.

Collisions in the present DSMC code are modeled by the variable-hard-sphere molecular model [18] and the no time counter collisional sampling technique [19]. The Borgnakke–Larsen statistical model [20] is used to repartition energy among the internal and translation modes after a collision. Simulations are performed using a nonreacting gas model consisting of two chemical species, N_2 and O_2. The vibrational temperature is controlled by the distribution of energy between the translational and rotational modes after an

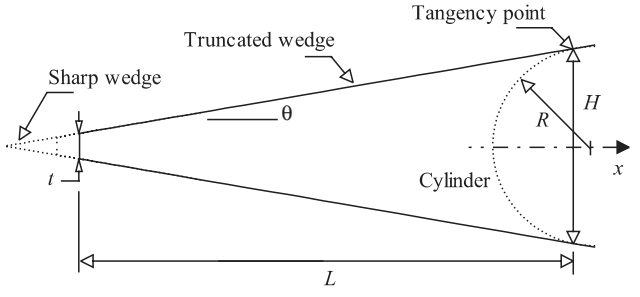

Fig. 1 Drawing illustrating the leading-edge geometry.

DSMC Algorithm

1. Initialize cells according to initial conditions;
2. Main time sptepping loop:
   a) Move particles according to their velocities;
   b) Index particles into cells;
   c) Select collision pairs and perform intermolecular collisions;
   d) Sample flow properites;
3. Average samples after establishing steady flow.

Fig. 2 DSMC algorithm.

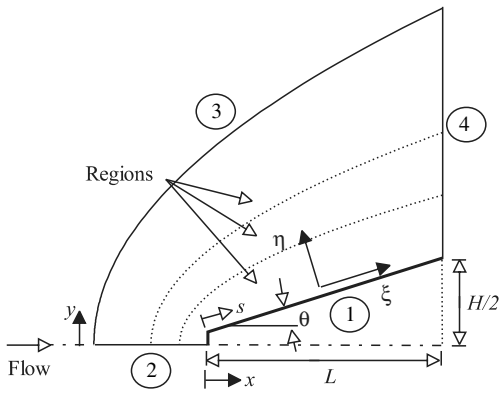

Fig. 3 Schematic view of the computational domain.

inelastic collision. The rates of rotational and vibrational relaxation are dictated by collisional numbers Z_R and Z_V, respectively. The collisional numbers are traditionally given as constants: 5 for rotational and 50 for vibrational.

IV. Computational Flow Domain and Grid

The computational domain used for the numerical treatment of the problem was divided into an arbitrary number of regions, which are subdivided into computational cells with dimensions that satisfy the DSMC computational requirements [21]. The cells are further subdivided into subcells, two subcells per cell in each coordinate direction. The cell provides a convenient reference for the sampling of the macroscopic flowfield properties, while the subcell is used to select possible collisional partners. A schematic view of the computational domain is depicted in Fig. 3. The advantage of the flow symmetry is taken into account, and molecular simulation is applied to one-half of a full configuration.

Referring to Fig. 3, side 1 is defined by the body surface. Diffuse reflection with complete thermal accommodation is the condition applied to this side. Side 2 is a plane of symmetry, and this plane is equivalent to a specular reflecting boundary. Side 3 is the freestream side through which simulated molecules enter and exit. Finally, the flow at the downstream outflow boundary, side 4, is predominantly supersonic and vacuum condition [17] is specified. At this boundary, simulated molecules can only exit.

The numerical accuracy in DSMC method depends on the cell size chosen, on the time step as well as on the number of particles per computational cell. In the DSMC code, the linear dimensions of the cells should be small in comparison with the length scale of the macroscopic flow gradients normal to streamwise directions, which means that the cell dimensions should be in the order of or smaller than the local mean free path [22,23]. The time step should be chosen to be sufficiently small in comparison with the local mean collisional time [24,25]. In general, the total simulation time, discretized into time steps, is based on the physical time of the real flow. Finally, the number of simulated particles has to be large enough to make statistical correlations between particles insignificant.

A grid independence study was made with three different structured meshes in each coordinate direction (see Fig. 3). The effect of altering the cell size in the ξ direction was investigated with grids of 50 (coarse), 100 (standard), and 150 (fine) cells, and 60 cells in the η direction. In analogous fashion, an examination was made in the η direction with grids of 30 (coarse), 60 (standard), and 90 (fine) cells, and 100 cells in the ξ direction. Each grid was made up of nonuniform cell spacing in both directions. The effect (not shown) of changing the cell size in both directions on the heat transfer, pressure, and skin friction coefficients was rather insensitive to the range of cell spacing considered, indicating that the standard grid, 100×60 cells, is essentially grid independent.

A similar examination was made for the number of molecules. The standard grid, 100×60 cells, corresponds to, on average, a total of 190,000 molecules. Two new cases using the same grid, corresponding to 104,000 and 283,000 molecules in the entire computational domain, were investigated. As the three cases presented approximately the same results (not shown) for the heat transfer, pressure, and skin friction coefficients, the standard grid, with a total of 190,000 molecules, is enough for the computation of the aerodynamic surface quantities. A discussion of these effects on the aerodynamic surface quantities is described in detail in Santos [2,3].

V. Freestream and Flow Conditions

Freestream and flow conditions used in the present calculations are those given by Santos [3] and summarized in Table 1. In addition, gas properties [17] are tabulated in Table 2. The freestream velocity V_∞ was assumed to be constant at 1487, 2379, and 3568 m/s, which correspond to freestream Mach number M_∞ of 5, 8, and 12, respectively. The translational and vibrational temperatures in the freestream are in equilibrium at 220 K, and the leading-edge surface has a constant temperature T_w of 880 K for all cases considered.

The overall Knudsen numbers Kn_t, defined as the ratio of the freestream mean free path λ_∞ to the leading-edge thickness t, corresponds to 100, 10, and 1 for leading-edge thickness t/λ_∞ of 0.01, 0.1, and 1, respectively. The Reynolds number Re_t covers the range from 0.193 to 19.3, based on conditions in the undisturbed stream with leading-edge thickness t as the characteristic length.

VI. Computational Procedure

The flowfield properties upstream and adjacent to the leading edge of a body are affected by molecules reflected from the edge region. The degree of the effect is in part conditioned by the edge geometry. In an effort to understand the influence of the flowfield on the behavior of the aerodynamic surface properties at the vicinity of the leading-edge nose, the present account will employ a procedure [26]

Table 1 Freestream and flow conditions

Parameter	Value	Unit
Temperature T_∞	220.0	K
Pressure p_∞	5.582	N/m^2
Density ρ_∞	8.753×10^{-5}	kg/m^3
Viscosity μ_∞	1.455×10^{-5}	Ns/m^2
Number density n_∞	1.8209×10^{21}	m^{-3}
Mean free path λ_∞	9.03×10^{-4}	m

Table 2 Gas properties

Parameter	O_2	N_2	Unit
Molecular mass m	5.312×10^{-26}	4.65×10^{-26}	kg
Molecular diameter d	4.010×10^{-10}	4.11×10^{-10}	m
Mole fraction χ	0.237	0.763	——
Viscosity index, ω	0.77	0.74	——

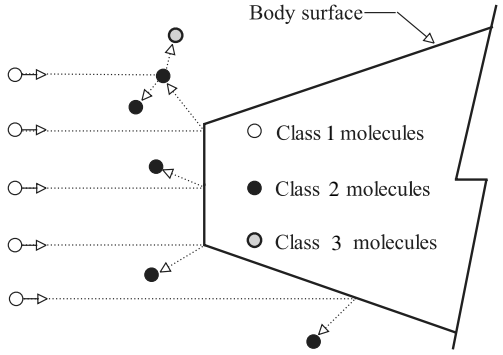

Fig. 4 Drawing illustrating the classification of molecules.

based on the physics of the particles. In this respect, the entire flowfield is assumed to consist of three distinct classes of molecules: those molecules from the freestream that have not been affected by the presence of the leading edge are denoted as class 1 molecules; those molecules that, at some time in their past history, have collided and been reflected from the leading-edge surface are denoted as class 2 molecules; and those molecules that have been indirectly affected by the presence of the leading edge are defined as class 3 molecules. Figure 4 illustrates the definition for the molecular classes.

It is assumed that the class 1 molecule changes to class 3 molecule when it collides with class 2 or class 3 molecule. A class 1 or class 3 molecule is progressively transformed into class 2 molecule when it interacts with the body surface. Also, a class 2 molecule remains class 2 regardless of subsequent collisions and interactions. Hence, the transition from class 1 molecules to class 3 molecules may represent the shock wave, and the transition from class 3 to class 2 may define the boundary layer.

VII. Computational Results and Discussion

In the present study, effort is directed to understand the flowfield behavior and its influence on the heat transfer coefficient at the vicinity of the frontal-face/afterbody junction. Therefore, this section will discuss differences in the heat transfer coefficient behavior due to variations in the leading-edge thickness and to compare to that by considering free-molecular flow. To present the problem coherently, it is necessary to repeat the heat transfer analysis of previous publications to some extent. In doing so, the present approach begins with the results of Santos [3] in which, for any particular reasons, the heat transfer coefficient was above that predicted by the free-molecular-flow equations.

The heat transfer coefficient C_h is defined as being

$$C_h = \frac{q_w}{\frac{1}{2}\rho_\infty V_\infty^3} \tag{1}$$

where the heat flux q_w to the body surface is calculated by the net energy fluxes of the molecules impinging on the surface. A flux is regarded as positive if it is directed toward the surface. The heat flux q_w is related to the sum of the translational, rotational, and vibrational energies of both incident and reflected molecules, as defined by

$$q_w = q_i + q_r = \sum_{j=1}^{N}\left[\frac{1}{2}m_j c_j^2 + e_{Rj} + e_{Vj}\right]_i + \sum_{j=1}^{N}\left[\frac{1}{2}m_j c_j^2 + e_{Rj} + e_{Vj}\right]_r \tag{2}$$

where N is the number of molecules colliding with the surface by unit time and unit area, m is the mass of the molecules, c is the velocity of the molecules, e_R and e_V are the rotational and vibrational energies, respectively, and subscripts i and r refer to incident and reflect molecules.

Distributions of the heat transfer coefficient C_h along the frontal and afterbody surfaces are illustrated in Figs. 5 and 6, respectively, parameterized by the freestream Mach number for leading-edge thickness t/λ_∞ of 0.01, 0.1, and 1, which correspond to thickness Knudsen numbers Kn_t of 100, 10, and 1, respectively. In this set of plots, Figs. 5a–5c correspond to the heat transfer coefficient C_h along

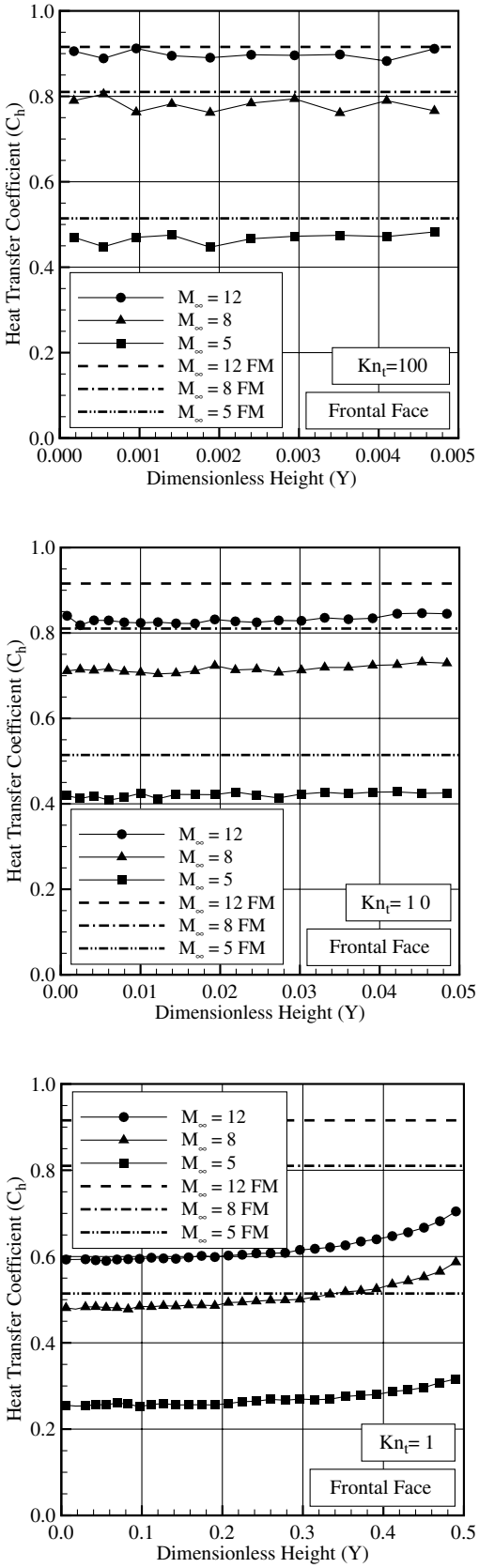

Fig. 5 Distributions of the heat transfer coefficient C_h along the frontal surface of the leading edges as a function of the freestream Mach number for thickness Knudsen numbers Kn_t of a) 100, b) 10, and c) 1.

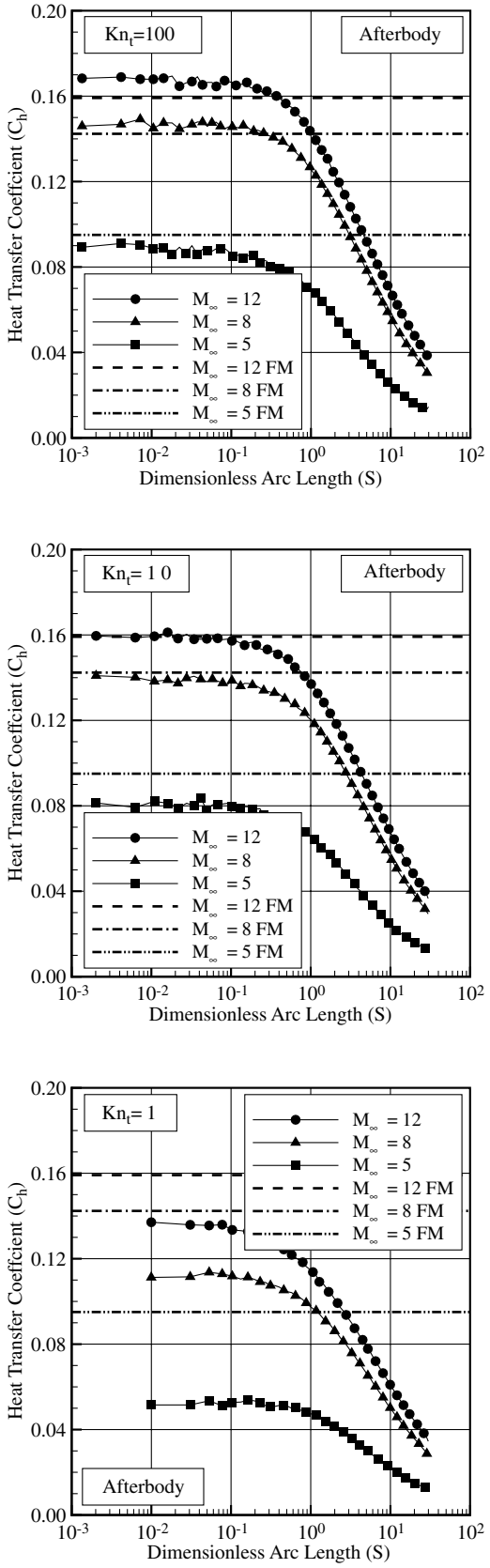

Fig. 6 Distributions of the heat transfer coefficient C_h along the afterbody surface of the leading edges as a function of the freestream Mach number for thickness Knudsen numbers Kn_t of a) 100, b) 10, and c) 1.

the frontal face as a function of the dimensionless height $Y(\equiv y/\lambda_\infty)$, measured from the stagnation point up to the shoulder of the wedge. Figs. 6a–6c correspond to the heat transfer coefficient C_h along the afterbody surface of the wedge as a function of the dimensionless arc length $S(\equiv s/\lambda_\infty)$, measured from the shoulder of the leading edge. For purpose of comparison, Figs. 5 and 6 display the free-molecular-flow limit value for the heat transfer coefficient by assuming collisionless flow.

Free-molecular flow or collisionless flow is the limiting case in which the Knudsen number tends to infinity. It is the subdivision of rarefied gas dynamics corresponding to the lowest densities, therefore with very high mean free paths or with very small characteristic dimensions. Analytical expressions for number flux, pressure coefficient, heat transfer coefficient, and skin-friction coefficient have been derived [17] by assuming that the flow past the surface element is in Maxwellian equilibrium with the freestream number density n_∞, temperature T_∞, macroscopic velocity V_∞ inclined at an angle of incidence α to the unit normal vector to the surface element, and diffuse reflection. However, the body slope angle θ is related to the angle of incidence α of the element surface by $\pi/2 - \alpha$, and this angle seems to be more appropriate for this work. In this fashion, the heat transfer coefficient when considering free-molecular flow is given by the following expression [17]:

$$C_h = \frac{1}{2\sqrt{\pi}\beta_\infty^3}\left\{\left[\beta_\infty^2 + \frac{\gamma}{\gamma-1} - \frac{\gamma+1}{2(\gamma-1)}\frac{T_w}{T_\infty}\right][e^{-\chi^2} + \sqrt{\pi}\chi(1+erf\chi)] - \frac{1}{2}e^{-\chi^2}\right\} \tag{3}$$

where γ is the specific heat ratio, β_∞ is the speed ratio of the freestream defined by $V_\infty\sqrt{2RT_\infty}$, and $\chi = \beta_\infty \sin\theta$ with R is the gas constant.

By considering free-molecular flow, the heat transfer coefficient C_h to the frontal surface predicted by Eq. (3) is 0.514, 0.810, and 0.916 for freestream Mach number M_∞ of 5, 8, and 12, respectively. For the afterbody surface, the free-molecular-flow values are 0.095, 0.142, and 0.159 for M_∞ of 5, 8, and 12, respectively.

According to Figs. 5 and 6, it is seen that the heat transfer coefficient C_h changes on the frontal and afterbody surfaces of the wedge with increasing not only the freestream Mach number but also the frontal-face thickness. As the freestream Mach number increases from 5 to 12, the kinetic energy of the freestream molecules increases. Consequently, the heat flux to the body surface increases. An understanding of this behavior can be gained by analyzing Eq. (2). The incident component of the velocity c of the molecules is a function of the freestream Mach number. However, the reflected component of the molecular velocity is not a function of the freestream Mach number. Because of the diffuse reflection model, the reflected component of the molecular velocity is obtained from a Maxwellian distribution that takes only into account for the temperature of the body surface, which has the same value for the freestream Mach number range investigated. It should also be emphasized that the number of molecules colliding with the surface by unit time and unit area N, which appears in Eq. (2), is the same for the incident and reflected components of the heat transfer coefficient C_h. Nevertheless, N increases on the frontal and afterbody surfaces of the leading edges with increasing the freestream Mach number and the frontal-face thickness, as is subsequently seen. Particular attention is paid to the heat transfer coefficient at the vicinity of the shoulder for the bluntest case investigated, $Kn_t = 1(t/\lambda_\infty = 1)$. For the $Kn_t = 1$ case, the heat transfer coefficient C_h increases at the vicinity of the shoulder, in contrast to the aerodynamically sharp leading-edge cases investigated, $Kn_t = 10$ and 100. This behavior would be also expected because the velocity of the molecules increases at the vicinity of the shoulder, where the flow is allowed to expand. In addition, the contribution of the translational energy to the net heat flux varies with the square of the velocity of the molecules, as shown in Eq. (2).

Referring to Fig. 6a, it is very encouraging to observe that the heat transfer coefficient C_h on the afterbody surface, at the vicinity of the frontal-face/afterbody junction, is above that predicted by the free-molecular-flow equations. It should be mentioned in this context that this behavior has been observed on the surface properties at the vicinity of the nose for sharp leading edges, such as flat plate, wedge,

and cone. As an illustrative example, Vidal and Bartz [6] observed from their experimental investigations on flat plates and wedges that the heat transfer rate approached the free-molecular limit from above, whereas those obtained at large wedge angles approached from below. According to them, for the particular conditions on the experiment, a 2 deg wedge angle appeared to be the crossover point where the approach to the free-molecular limit was at the level of the free-molecular limit. Their wedge flows were produced by pitching the flat-plate model to various compression angles.

With this perspective in mind, Fig. 6 reveals the presence of two possible crossover points. The first one is related to the freestream Mach number effect on the thickness Knudsen number Kn_t of 100, as illustrated in Fig. 6a. It is clearly seen that for freestream Mach numbers of 12 and 8, the heat transfer coefficient C_h approaches the free-molecular-flow limit from above. Conversely, for freestream Mach number of 5, C_h approaches it from below. The second one is connected to the frontal-face thickness effect for freestream Mach numbers of 8 and 12. For thickness Knudsen number Kn_t of 100, as shown in Fig. 6a, the heat transfer coefficient C_h approaches from above, and for thickness Knudsen number Kn_t of 1, C_h approaches from below, as shown in Fig. 6c. Based on Vidal and Bartz [6], for the first case, the crossover point is between freestream Mach numbers of 8 and 5. For the second case, the leading edge defined by thickness Knudsen number Kn_t of 10 appears to be the crossover point, where the approach to the free-molecular limit is at the level of the free-molecular limit.

This behavior is explained by the fact that collision of the oncoming freestream molecules (class 1 molecules); therefore, high-velocity molecules, with the molecules emitted from the body surface (class 2 molecules), will on average cause at least some of the oncoming molecules to be reflected onto the body surface, thereby increasing the heat transfer rate over the free-molecular value owing to the increased energy. This result is in contrast to the rarefied flow past blunt leading edge, Kn_t of 1, as shown in Fig. 6c. For the blunt leading edge, the effect of collisions of the oncoming freestream molecules with those emitted from the surface will be to deflect some of the incident molecules from the surface, thereby reducing the heat transfer rate relative to the free-molecular value.

In what follows, it proves helpful to present the number flux to the body surface. The number flux N is calculated by sampling the molecules impinging on the surface by unit time and unit area. The impact of the number flux on the frontal and afterbody surfaces due to variations on the frontal-face thickness is demonstrated in Figs. 7 and 8, respectively, for thickness Knudsen numbers Kn_t of 100, 10, and 1. In this set of plots, N_f stands for the number flux N normalized by $n_\infty V_\infty$, where n_∞ is the freestream number density and V_∞ is the freestream velocity. As a basis of comparison, these figures display the free-molecular-flow limit value for the dimensionless number flux by assuming collisionless flow. In this fashion, the dimensionless number flux by considering free-molecular flow is given by the following expression [17]:

$$\frac{N}{n_\infty V_\infty} = \frac{1}{2\sqrt{\pi}\beta_\infty}[e^{-\chi^2} + \sqrt{\pi}\chi(1 + erf\chi)] \tag{4}$$

By analyzing Eq. (4), the dimensionless number flux for free-molecular flow tends to $\sin\theta$, as the freestream speed ratio $\beta_\infty \to \infty$. As the freestream Mach number increases from 5 to 12, the freestream speed ratio β_∞ increases from 4.18 to 9.44. For the frontal surface, with a slope angle of 90 deg, $N_f(\equiv N/n_\infty V_\infty) = 1$ for freestream Mach numbers of 5, 8, and 12. As a result, the dimensionless number flux for free-molecular flow becomes independent of the freestream speed ratio or freestream Mach number for the range investigated. This is related to the Mach number independence principle; it means that the flowfield becomes independent of Mach number if the Mach number is sufficiently large. For the afterbody surface, with a slope angle of 10 deg, the free-molecular value from Eq. (4) is 0.187, 0.176, and 0.174 for freestream Mach numbers of 5, 8, and 12, respectively.

Looking first at Figs. 7a–7c, it is clearly seen that the dimensionless number flux to the frontal surface increases by increasing the frontal-face thickness. This is an expected behavior since the leading-edge changes aerodynamically from a sharp to blunt one with increasing the frontal-face thickness. In addition, for thickness Knudsen number Kn_t of 100, the dimensionless number flux N_f to

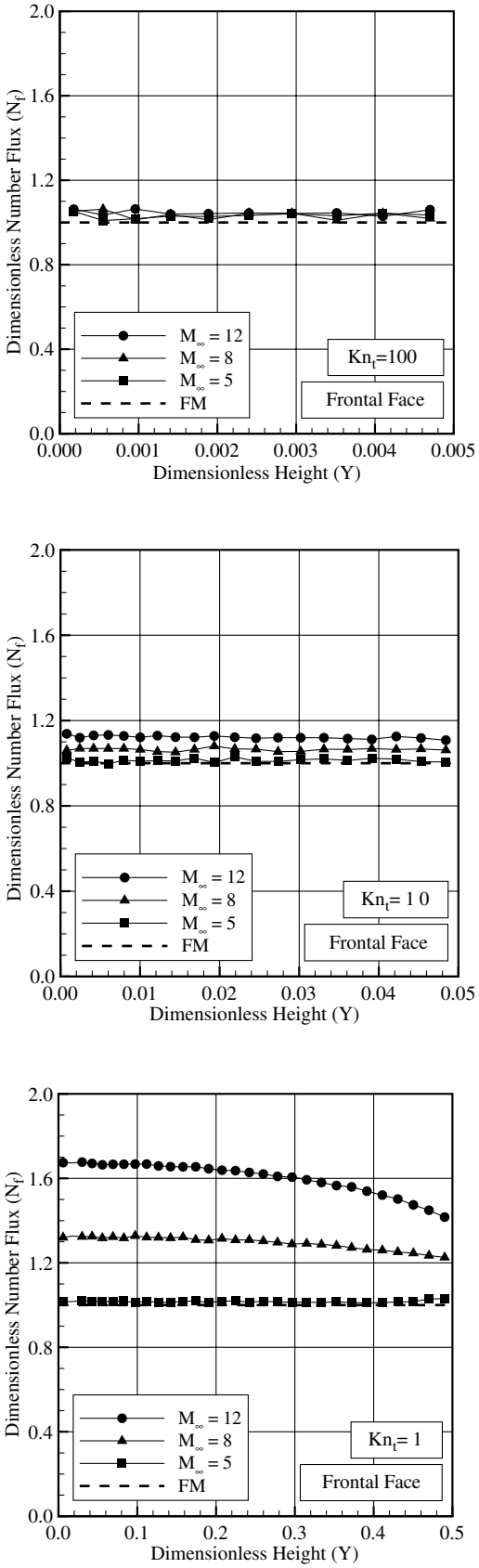

Fig. 7 Distributions of the dimensionless number flux N_f along the frontal surface of the leading edges as a function of the freestream Mach number for thickness Knudsen numbers Kn_t of a) 100, b) 10, and c) 1.

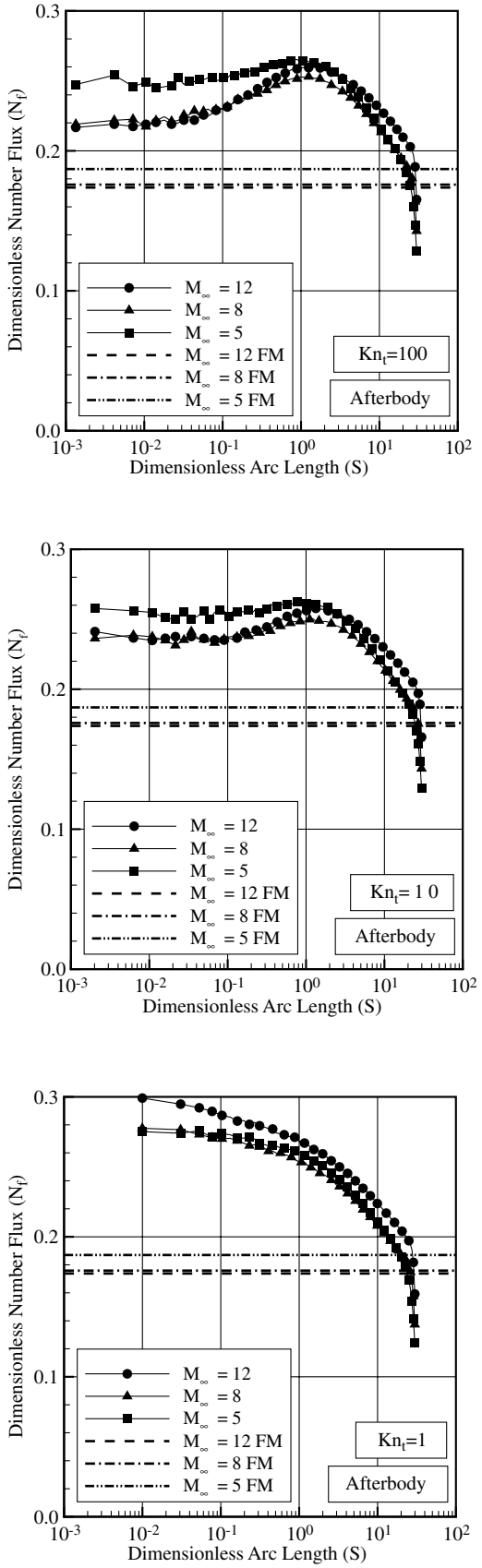

Fig. 8 Distributions of the dimensionless number flux N_f along the afterbody surface of the leading edges as a function of the freestream Mach number for thickness Knudsen numbers Kn_t of a) 100, b) 10, and c) 1.

the frontal surface approaches the limit value, $N/n_\infty V_\infty = 1$, obtained by Eq. (4).

Turning next to Figs. 8a–8c, it is observed that the dimensionless number flux at the vicinity of the frontal-face/afterbody junction is far from the limit value predicted by the free-molecular flow. It is also observed that the dimensionless number flux to the afterbody surface is one order of magnitude smaller than that to the frontal surface. Moreover, as mentioned earlier, as the frontal-face thickness increases, the leading edge becomes blunter and a rather different flow behavior is seen, as shown in Fig. 8c, where the general shape for the number flux related to $Kn_t = 1$ displays a different profile as compared to those presented by the $Kn_t = 10$ and 100 cases.

For the time being, it proves helpful to add in this context that the free-molecular-flow equations are obtained from the premise that there are no intermolecular collisions. Thus, incident flux to the surface can be treated separately from reflected flux, with fluxes of interest being mass, momentum, and energy. The incident flux is entirely unaffected by the presence of the surface. To elucidate the effect posed above, in the sense that collision of the oncoming freestream molecules (class 1) with the molecules emitted from the body surface (class 2) will on average cause at least some of the oncoming molecules to be reflected onto the body surface, thereby increasing the heat transfer rate over the free-molecular value, the simulation for the leading edge represented by $Kn_t = 100$ is again examined for freestream Mach numbers of 8 and 12, but this time the intermolecular collisions will not be take into account in the DSMC simulation. This procedure corresponds to skip the step 2c) listed in the DSMC algorithm illustrated in Fig. 2.

In this framework, Figs. 9 and 10 compare the simulation results for the distributions of heat transfer coefficient C_h and the dimensionless number flux N_f, respectively, by considering collisionless flow, with those yielded by the free-molecular-flow equations. As indeed is clear from these figures, the results obtained by the DSMC simulations are in excellent agreement with that yielded by the free-molecular-flow equations. It is thus firmly established that the heat transfer rate over the free-molecular value, as shown in Fig. 6a, is indeed directly related to the collision of two groups of molecules: the oncoming freestream molecules (class 1) and the molecules emitted from the body surface (class 2).

At this point, it is worth taking a closer look at the results from molecular class distributions. According to Fig. 4, the molecules are identified as classes 1, 2 and 3. As the flowfield is divided into cells, information on collisions between the molecules may be stored, and interesting features can be drawn from the results. In this sense, for three classes of molecules, six pairs of collisions are possible: collisions of class 1 with class 1, 2 vs 2, 1 vs 3, 2 vs 2, 2 vs 3, and 3 vs 3. Of particular interest in the present account are the collisions between molecules 1 vs 2 and 2 vs 3 taking place in the cells adjacent to the body surface. In this way, Figs. 11 and 12 illustrate the distributions of collisions of class 1 vs class 2 and class 2 vs class 3, respectively, for thickness Knudsen numbers Kn_t of 100, 10, and 1 with freestream Mach number of 12. In this set of figures, Y and X are the height y and length x, respectively, normalized by the freestream mean free path λ_∞. In addition, the contour scale represents the ratio of the number of collisions for the specific pair to the total number of collisions inside the cell, after the establishment of the steady state. As a result, the light gray portions of the plots show regions of the flow in which collisions for that particular pair of molecular classes are not so significant. In contrast, dark gray regions correspond to those regions in which collisional frequency is representative.

Looking at Fig. 11a, for the $Kn_t = 100$ case, it is seen that collisions between molecules of class 1 with those of class 2 are responsible from 20 to 25% of the total number of collisions taking place in the cells adjacent to the frontal surface and to the afterbody surface along a distance of half-freestream mean free path λ_∞, measured from the frontal-face/afterbody junction. Basically, the distance where the heat transfer coefficient is above the free-molecular limit, as shown in Fig. 6a. In contrast, for the $Kn_t = 1$ case, collisions of class 1 vs class 2 taking place in the cells adjacent to the leading-edge surface contributes to only 5% of the total number of

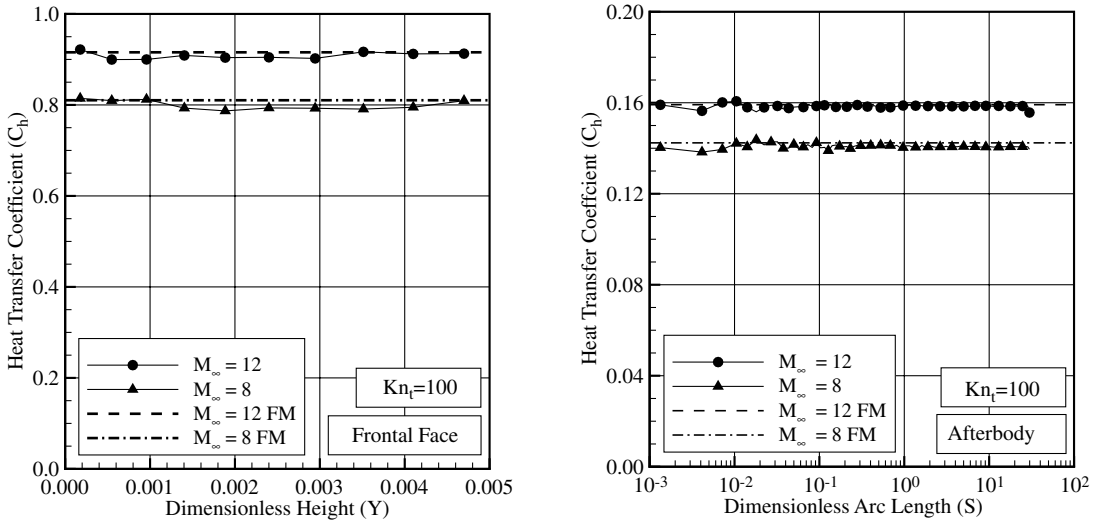

Fig. 9 Distributions of the heat transfer coefficient C_h along the a) frontal and b) afterbody surface of the leading edge as a function of the freestream Mach number for thickness Knudsen numbers Kn_t of 100.

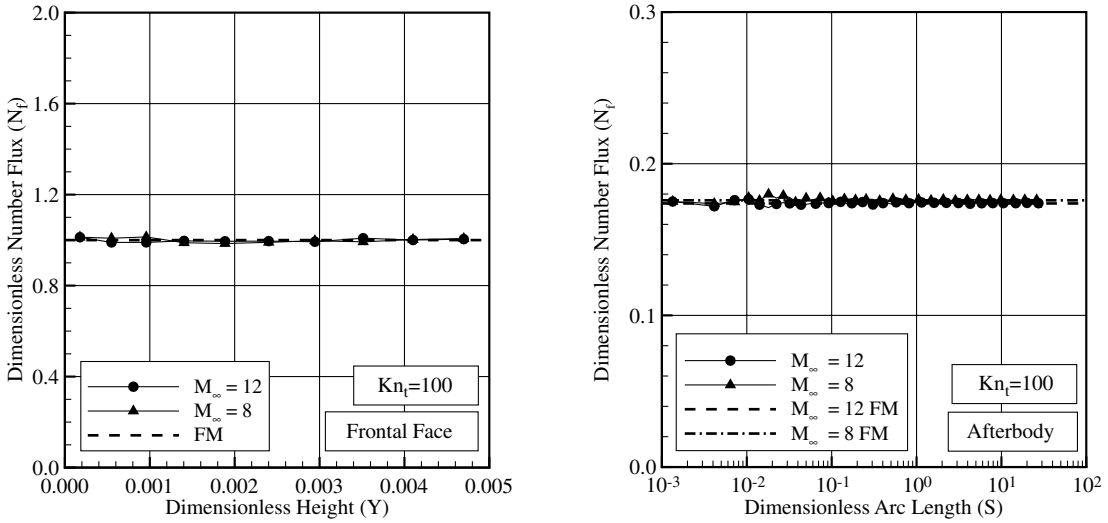

Fig. 10 Distributions of the dimensionless number flux N_f along the a) frontal and b) afterbody surfaces of the leading edge as a function of the freestream Mach number for thickness Knudsen numbers Kn_t of 100.

collisions, as illustrated in Fig. 11c. Therefore, it is seen that as the leading edge becomes blunter by decreasing the thickness Knudsen number Kn_t, the region where collisions of class 1 vs class 2 are maximum moves away from the frontal surface of the leading edges.

Turning to Fig. 12a, for the $Kn_t = 100$ case, it is observed that collisions between molecules of class 2 with those of class 3 represent around only 6% of the total number of collisions occurring adjacent to the afterbody surface at the vicinity of the frontal-face/afterbody junction. Conversely, for the $Kn_t = 1$ case, collisions class 2 vs class 3 contribute to about 15%, as shown in Fig. 12c.

Flow peculiarities, assessed from the molecular class procedure, are presented in the results that follow. As the molecules are identified by class, it proves instructive to determine the contribution of each molecular class to the total number flux and to the net heat flux to the leading-edge surface.

In this sense, Figs. 13 and 14 display the contribution of the molecules, identified by the classes, with the number flux and with the heat transfer coefficient, respectively, along with the afterbody surface of the leading edges. In this set of diagrams, $N_{f,1}$, $N_{f,2}$, and $N_{f,3}$ stand for the ratio of the number flux of molecular classes 1, 2, and 3, respectively, to the total number flux N_f. In addition, $N_{f,1}$, $N_{f,2}$, and $N_{f,3}$ are represented by triangle, square, and circle symbols, respectively. Similarly, $C_{h,1}$, $C_{h,2}$, and $C_{h,3}$ represent the heat transfer coefficient ratio of molecular classes 1, 2, and 3 to the net heat transfer coefficient C_h. Open symbols refer to freestream Mach number of 5, and filled symbols represent freestream Mach number of 12.

According to Figs. 13a–13c, it may be recognized that the behavior of the molecules colliding to the afterbody surface depends not only on the freestream Mach number but also on the thickness Knudsen number Kn_t. For the sharpest leading edge investigated, $Kn_t = 100$, molecules of classes 1, 2, and 3 contribute 58, 12, and 30%, respectively, to the total number flux for freestream Mach number of 5 at the vicinity of the wedge shoulder. By increasing the freestream Mach number to 12, the contribution changes to 71, 12, and 17% for classes 1, 2 and 3, respectively. Consequently, as class 1 molecules are molecules with high velocities, the heat transfer coefficient for Mach number of 12 will be higher than that for Mach number of 5, as shown in Fig. 6. For the bluntest leading edge, $Kn_t = 1$, a different behavior is clearly observed in the contribution of the molecular classes to the number flux, as illustrated in Fig. 13c. The total number flux is composed of 5, 30, and 65% of molecules of classes 1, 2, and 3, respectively, for freestream Mach number of 5, at the vicinity of the frontal-face/afterbody junction. In contrast, these numbers change to around 11, 41, and 48%, respectively, for Mach number of 12.

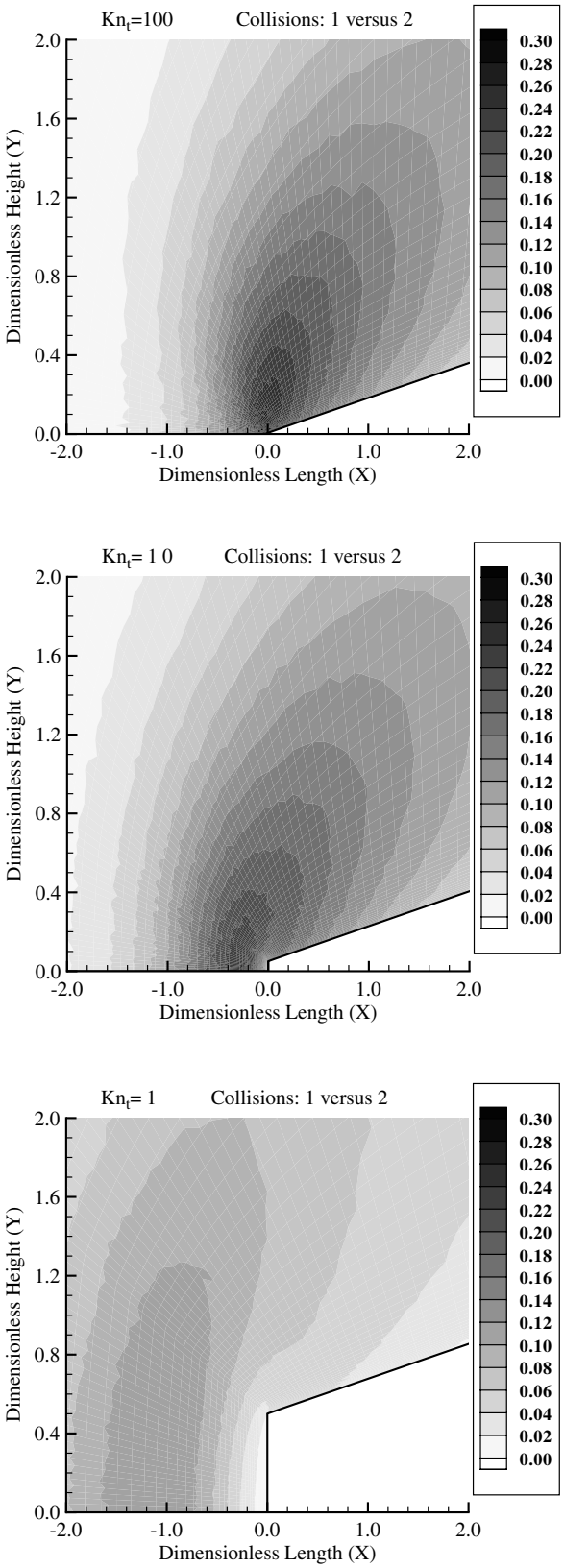

Fig. 11 Distributions of collisions between molecules of class 1 with class 2 at the vicinity of the leading edges for thickness Knudsen numbers Kn_t of a) 100, b) 10, and c) 1, and freestream Mach number of 12.

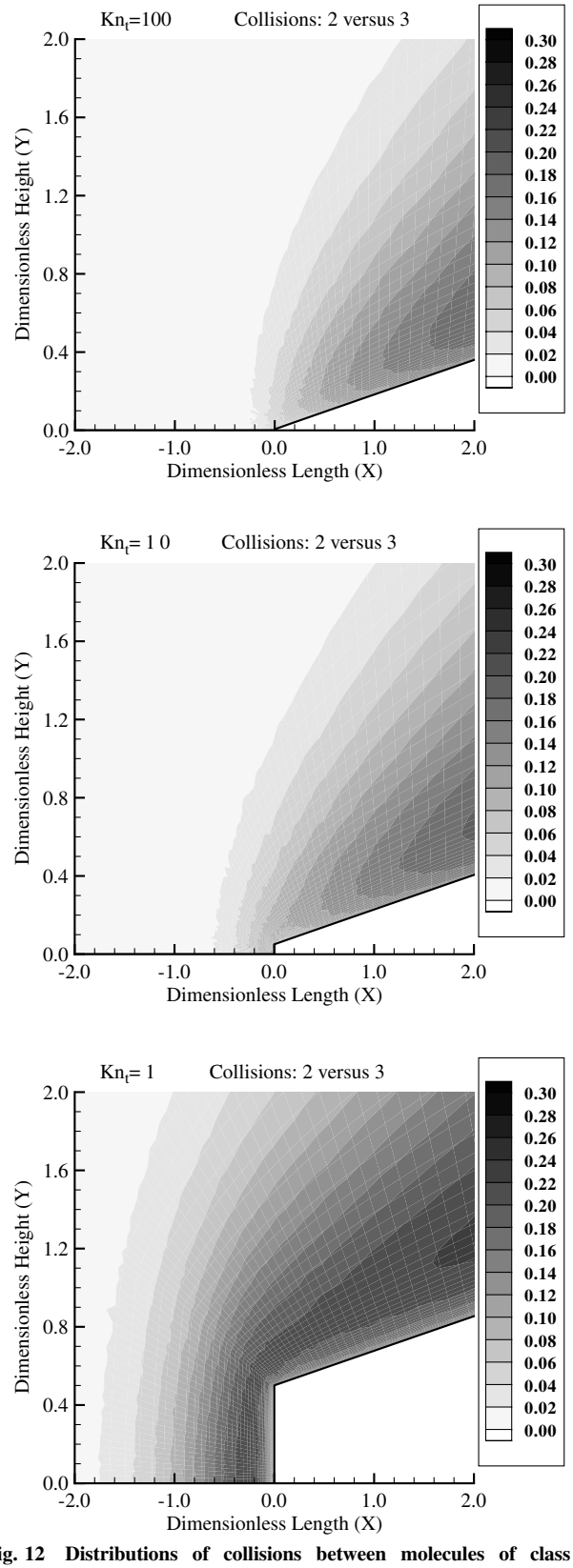

Fig. 12 Distributions of collisions between molecules of class 2 with class 3 at the vicinity of the leading edges for thickness Knudsen numbers Kn_t of a) 100, b) 10, and c) 1, and freestream Mach number of 12.

Still referring to Figs. 13a–13c, it is very encouraging to observe that for Kn_t of 100 and 10, the contribution of the molecular class 3 reaches a pick value at station $S = 2$. Conversely, for Kn_t of 1, the contribution of the molecular class 3 is large at the vicinity of the shoulder and decreases monotonically along the afterbody surface. Therefore, it may be inferred in passing that this behavior for Kn_t of 100 and 10 is associated to a sharp or aerodynamically sharp leading edge, whereas for Kn_t of 1, it is related to a blunt leading edge.

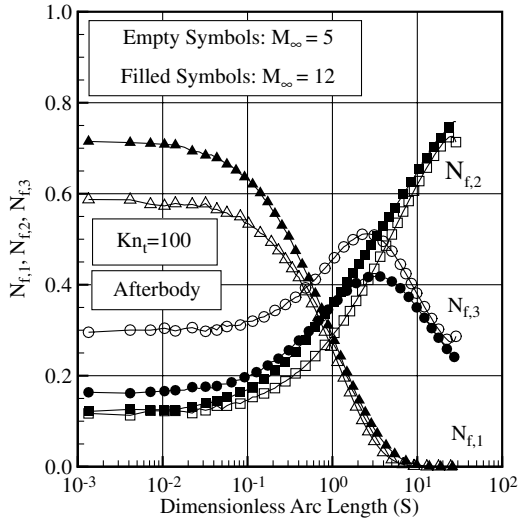

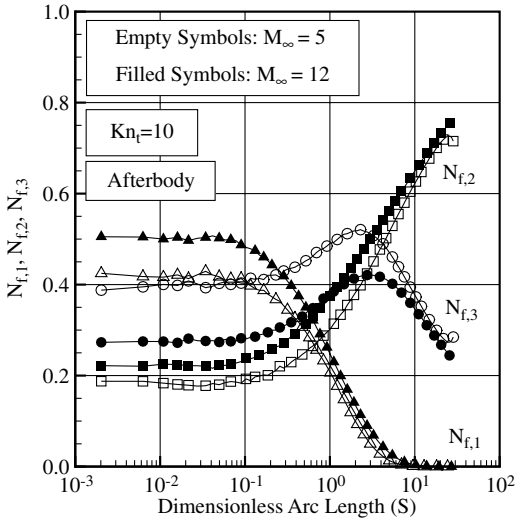

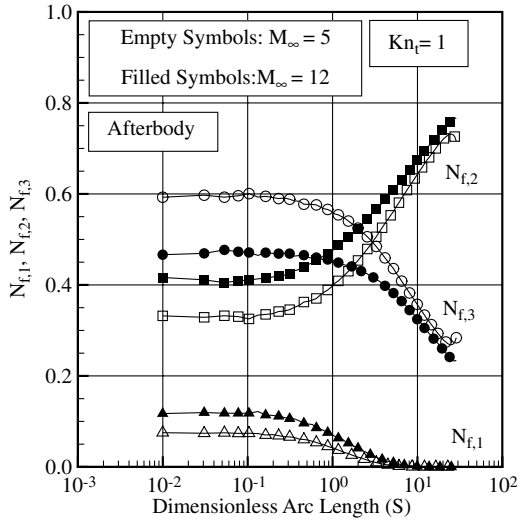

Fig. 13 Contribution of the molecules of classes 1, 2, and 3 to the number flux along the afterbody surface of the leading edges for thickness Knudsen numbers Kn_t of a) 100, b) 10, and c) 1.

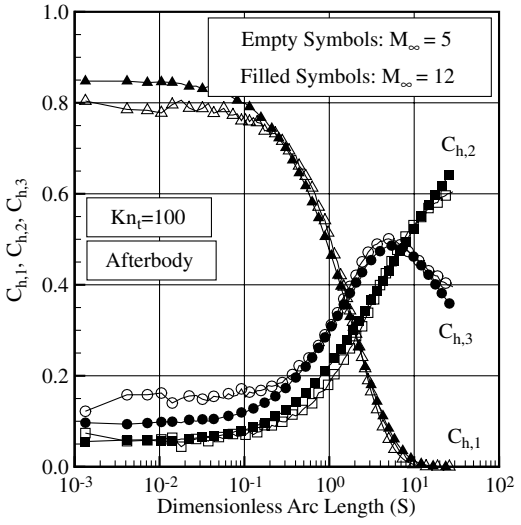

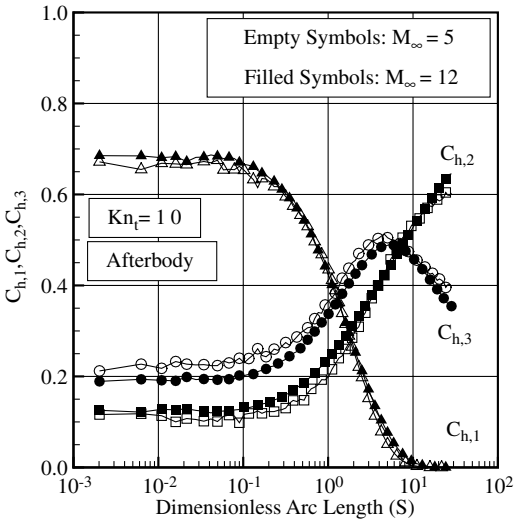

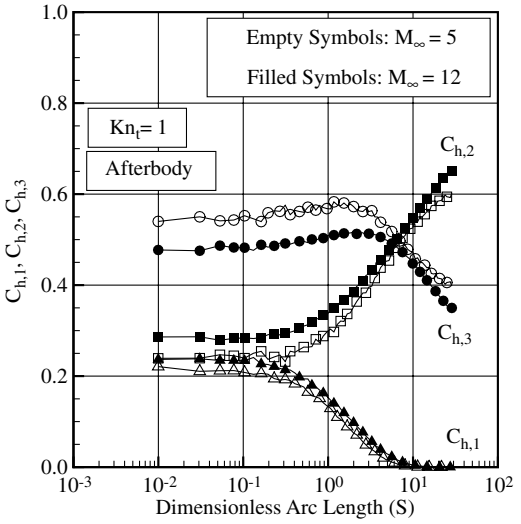

Fig. 14 Contribution of the molecules of classes 1, 2, and 3 to the heat transfer coefficient along the afterbody surface of the leading edges for thickness Knudsen numbers Kn_t of a) 100, b) 10, and c) 1.

According to Figs. 14a–14c, it is apparent that as Kn_t decreases from 100 to 1 (that is, as the leading-edge shape changes from sharp or aerodynamically sharp to blunt one), the contribution of the class 1 molecules to the heat flux, at the vicinity of the shoulder, dramatically decreases and the contribution of the classes 2 and 3 increases, as would be expected.

VIII. Conclusions

Numerical simulations of a rarefied hypersonic flow over truncated wedge have been performed by using the DSMC method. The simulations provided information concerning the behavior of number flux and the heat transfer coefficient along the frontal and afterbody surfaces.

Compressibility effects and the frontal-face thickness impact on the number flux and on the heat transfer coefficient were investigated for a representative range of parameters. The freestream Mach number varied from 5 to 12. In addition to that, the frontal-face thickness ranged from 0.01 to 1 of the freestream mean free path, with corresponding thickness Knudsen numbers from 100 to 1. Cases considered in this study covered the hypersonic flow from the transitional-flow regime to the free-molecular-flow regime.

It was found that the heat transfer rate for the smallest frontal-face thickness case approached the free-molecular limit from above, whereas that obtained for the largest frontal-face thickness case approached from below. According to the results, for the conditions on the investigation, there is a particular frontal-face thickness that represents the crossover point, where the approach to the free-molecular limit is at the level of the free-molecular limit.

By using a model that classifies the molecules in three distinct classes: undisturbed freestream, reflected, and scattered, this behavior on the heat transfer coefficient was investigated in detail. For the conditions investigated, the analysis showed that even for the smallest frontal-face thickness case, which corresponds to thickness Knudsen number of 100, the molecules reflecting from the frontal face interacted with freestream molecules and affected the heat transfer coefficient. As a result, the heat transfer coefficient approach to the free-molecular limit is above the level of the free-molecular limit.

References

[1] Nonweiler, T. R. F., "Aerodynamic Problems of Manned Space Vehicles," *Journal of the Royal Aeronautical Society*, Vol. 63, Sept. 1959, pp. 521–528.

[2] Santos, W. F. N., "Flat-Faced Leading-Edge Effects in Low-Density Hypersonic Wedge Flow," *Journal of Spacecraft and Rockets*, Vol. 42, No. 1, 2005, pp. 22–29. doi:10.2514/1.4907

[3] Santos, W. F. N., "Effects of Compressibility on Aerodynamic Surface Quantities over Low-Density Hypersonic Wedge Flow," *Journal of the Brazilian Society of Mechanical Sciences and Engineering*, Vol. 28, No. 3, 2006, pp. 362–372. doi:10.1590/S1678-58782006000300015

[4] Santos, W. F. N., "Bluntness Impact on Lift-to-Drag Ratio of Hypersonic Wedge Flow," *Journal of Spacecraft and Rockets*, Vol. 46, No. 2, 2009, pp. 329–339. doi:10.2514/1.41387

[5] Pan, Y. S. and Probstein, R. F., "Rarefied-Flow Transition at a Leading Edge," *Fundamental Phenomena in Hypersonic Flow*, Cornell Univ. Press, Ithaca, NY, 1965, pp. 259–309.

[6] Vidal, R. J., and Bartz, J. A., "Experimental Studies of Low-Density Effects in Hypersonic Wedge Flows," *Rarefied Gas Dynamics, Advance in Applied Mechanics*, Academic Press, New York, Vol. 1, Suppl. 3, 1965, pp. 467–486.

[7] Bird, G. A., "Aerodynamic Properties of Some Simple Bodies in the Hypersonic Transition Regime," *AIAA Journal*, Vol. 4, No. 1, 1966, pp. 55–60. doi:10.2514/3.3384

[8] McCroskey, W. J., Bogdonoff, S. M., and McDougall, J. G., "An Experimental Model for the Sharp Flat Plate in Rarefied Hypersonic Flow," *AIAA Jounal*, Vol. 4, No. 9, 1966, pp. 1580–1587. doi:10.2514/3.55283

[9] McCroskey, W. J., Bogdonoff, S. M., and Genchi, A. P., "Leading Edge Flow Studies of Sharp Bodies in Rarefied Hypersonic Flow," *Rarefied Gas Dynamics, Advance in Applied Mechanics*, Academic Press, New York, Vol. 2, Suppl. 4, 1967, pp. 1047–1066.

[10] Huang, A. B., and Hartley, D. L., "Kinetic Theory of the Sharp Leading Edge Problem in Supersonic Flow," *Physics of Fluids*, Vol. 12, No. 1, 1969, pp. 96–108. doi:10.1063/1.1692299

[11] Huang, A. B., and Hartley, D. L., "Supersonic Leading Edge Problem According to the Ellipsoidal Model," *Physics of Fluids*, Vol. 13, No. 2, 1970, pp. 309–317. doi:10.1063/1.1692921

[12] Vogenitz, F. W., and Takata, G. Y., "Rarefied Hypersonic Flow About Cones and Flat Plates by Monte Carlo Simulation," *AIAA Journal*, Vol. 9, No. 1, 1971, pp. 94–100. doi:10.2514/3.6128

[13] Huang, A. B., Hwang, P. F., Giddens, D. P., and Srinivasan, "High Speed Leading Edge Problem," *Physics of Fluids*, Vol. 16, No. 6, 1973, pp. 814–824. doi:10.1063/1.1694433

[14] Pullin, D. I., and Harvey, J. K., "A Numerical Simulation of the Rarefied Hypersonic Flat-Plate Problem," *Journal of Fluid Mechanics*, Vol. 78, No. 4, 1976, pp. 689–707. doi:10.1017/S0022112076002693

[15] Dogra, V. K., "Rarefied Flow Past a Flat Plate at Incidence," *Rarefied Gas Dynamics: Theoretical and Computational Techniques*, edited by E. P. Muntz, D. P. Weaver, and D. H. Campbell, Vol. 118, Progress in Astronautics and Aeronautics, AIAA, New York, 1989, pp. 567–581.

[16] Cercignani, C., *The Boltzmann Equation and Its Applications*, Springer–Verlag, New York, 1988.

[17] Bird, G. A., *Molecular Gas Dynamics and the Direct Simulation of Gas Flows*, Oxford Univ. Press, Oxford, 1994.

[18] Bird, G. A., "Monte Carlo Simulation in an Engineering Context," *Progress in Astronautics and Aeronautics: Rarefied Gas Dynamics*, edited by S. S. Fisher, Vol. 74, Part 1, AIAA, New York, 1981, pp. 239–255.

[19] Bird, G. A., "Perception of Numerical Method in Rarefied Gasdynamics," *Rarefied Gas Dynamics: Theoretical and Computational Techniques*, edited by E. P. Muntz, D. P. Weaver, and D. H. Capbell, Vol. 118, Progress in Astronautics and Aeronautics, AIAA, New York, 1989, pp. 374–395.

[20] Borgnakke, C., and Larsen, P. S., "Statistical Collision Model for Monte Carlo Simulation of Polyatomic Gas Mixture," *Journal of Computational Physics*, Vol. 18, No. 4, 1975, pp. 405–420. doi:10.1016/0021-9991(75)90094-7

[21] Rieffel, M. A., "A Method for Estimating the Computational Requirements of DSMC Simulations," *Journal of Computational Physics*, Vol. 149, No. 1, 1999, pp. 95–113. doi:10.1006/jcph.1998.6140

[22] Alexander, F. J., Garcia, A. L., and, Alder, B. J., "Cell Size Dependence of Transport Coefficient in Stochastic Particle Algorithms," *Physics of Fluids*, Vol. 10, No. 6, 1998, pp. 1540–1542. doi:10.1063/1.869674

[23] Alexander, F. J., Garcia, A. L., and, Alder, B. J., "Erratum: Cell Size Dependence of Transport Coefficient is Stochastic Particle Algorithms," *Physics of Fluids*, Vol. 12, No. 3, 2000, pp. 731–731. doi:10.1063/1.870278

[24] Garcia, A. L., and, Wagner, W., "Time Step Truncation Error in Direct Simulation Monte Carlo," *Physics of Fluids*, Vol. 12, No. 10, 2000, pp. 2621–2633. doi:10.1063/1.1289691

[25] Hadjiconstantinou, N. G., "Analysis of Discretization in the Direct Simulation Monte Carlo," *Physics of Fluids*, Vol. 12, No. 10, 2000, pp. 2634–2638. doi:10.1063/1.1289393

[26] Santos, W. F. N., "Some Physical and Computational Aspects of Shock Wave over Power-Law Leading Edges," *Physics of Fluids*, Vol. 20, No. 1, 2008, Paper 016101–11. doi:10.1063/1.2831135

I. Boyd
Associate Editor